REPORT DOCUMENTATION PAGE

1. REPORT DATE (DD-MM-YYYY)	2. REPORT TYPE	3. DATES COVERED (From - To)
25-11-2008	Final Report	15 Feb. 2006 to 31 May 2008

4. TITLE AND SUBTITLE
Thermal Modeling of Millimeter Wave Energy and Heat Transfer in Skin

5a. CONTRACT NUMBER

5b. GRANT NUMBER
FA9550-06-1-0129

5c. PROGRAM ELEMENT NUMBER

6. AUTHOR(S)
Robert Blystone

5d. PROJECT NUMBER

5e. TASK NUMBER

5f. WORK UNIT NUMBER

7. PERFORMING ORGANIZATION NAME(S) AND ADDRESS(ES)
Trinity University
One Trinity Place
San Antonio, Texas 78212

8. PERFORMING ORGANIZATION REPORT NUMBER

9. SPONSORING / MONITORING AGENCY NAME(S) AND ADDRESS(ES)
USAF, AFRL
AFOSR
875 North Randolph Street
Suite 325, Room 3112
Arlington, VA 22203

10. SPONSOR/MONITOR'S ACRONYM(S)

11. SPONSOR/MONITOR'S REPORT NUMBER(S)
AFRL-OSR-VA-TR-2012-0065

12. DISTRIBUTION / AVAILABILITY STATEMENT
Unlimited

13. SUPPLEMENTARY NOTES

14. ABSTRACT
A thermal modeling algorithm was developed to predict the heat movement in rat skin continuously exposed for up to 60 minutes with 94 or 35 GHz millimeter radiofrequency radiation. The power densities applied were 50, 75, or 100 mW/cm^2 at either 23 or 33°C ambient temperature. The rat skin was viewed as stratified layers of dimensions 40μm epidermis, 100 μm papillary dermis, 600 μm reticular dermis, and 560 μm of hypodermis consisting of striated muscle, adipose, and connective tissue. 1.3 mm of skin depth encompasses the majority of tissue heat absorption at these frequencies and includes the dermal hypodermal interface where the greatest RFR-induced histological change took place. The six RFR exposure conditions encompass a range of rat thermal response ranging from tissue lesions and death to little response. Rats received isoflurane anesthesia, which in turn induced produced anesthesia hypothermia. Ways to adjust for this hypothermic response were sought in order to develop better verification procedures for the thermal model.

15. SUBJECT TERMS
Millimeter wave exposure, skin histology and pathology, thermal modeling, thermoregulation, heat transfer, thermal biology

16. SECURITY CLASSIFICATION OF:			17. LIMITATION OF ABSTRACT	18. NUMBER OF PAGES	19a. NAME OF RESPONSIBLE PERSON
a. REPORT	**b. ABSTRACT**	**c. THIS PAGE**	none	19	Robert Blystone
unclassified	unclassified	unclassified			**19b. TELEPHONE NUMBER** (include area code) 210 999 7243

Standard Form 298 (Rev. 8-98)
Prescribed by ANSI Std. Z39.18

20120918171

d. "Gene expression changes in liver and lung of rats exposed to sustained 35-GHZ millimeter wave energy. 28th Annual Meeting of the Bioelectromagnetics Society. Cancun, Mexico. (N.J. Millenbaugh, R. Sypniewska, C.C. Roth, V. Chan, C.Z. Cerna, B.J. Brott, J.L. Kiel, R.V. Blystone, and P.A. Mason) June 14, 2006.

e. "Correlating modeling data and real data: anesthesia and temperature depression." AFRL/HED Computational Biophysics Collaborative Workshop, San Antonio, Texas. (R.V. Blystone) August 11, 2006.

f. "Effects of long-duration millimeter wave exposure of rat skin: numerical and experimental results." 29th Annual Meeting of the Bioelectromagnetics Society, Kanazawa, Japan. (D.A. Nelson, R. Blystone, M.A. Shah, and J.L. Robles) June 12, 2007.

g. "Gene expression changes in rat skin following prolonged 35-GHz millimeter wave exposure." 29th Annual Meeting of the Bioelectromagnetics Society, Kanazawa, Japan. (W. Hubert, N. Millenbaugh, C. Roth, R. Sypniewska, V. Chan, J. Eggers, R. Blystone, J. Kiel, and P.A. Mason) June 14, 2007.

h. "RF and anesthesia hypothermia." 2007 Computational Biophysics Workshop. San Antonio, Texas. August 1, 2007. (R.V. Blystone)

i. "Anesthesia-induced hypothermia interaction with rat's heating response to 35 and 94 gigahertz exposure." 14th Annual Michaelson Research Conference. Portsmouth, NH. (R. Blystone, N. Almazora, J. Scudder, and A. MacDonald) August 4, 2007.

j. "Effect of weight-restriction on anesthetized rat skin histology and colonic temperature." Annual meeting of the Society for Integrative and Comparative Biology, San Antonio, Texas. (J. Scudder, D. Pulliam, R. Blystone, and I. Tovar) January 4, 2008.

3. **Scientific personnel supported by this grant along with their percent effort**:
   a. Noreen Almazora (Undergraduate Research Student) – 100% Summer 2006; 50% Fall 2006 and Spring 2007.
   b. Adam Back (Undergraduate Research Student) – 25% Spring 2006.
   c. Robert V. Blystone, Ph.D. (Principal Investigator) – 20% Spring 2006; 100% Summer 2006; 20% Fall 2006 and Spring 2007; 100% Summer 2007; 20% Fall 2007 and Spring 2008; 32% May 2008.
   d. Fernando Catalan (Research Technician I) – 100% February 20, 2006 to April 21, 2006.
   e. Florinda Galindo (Research Assistant) – 33% February 15, 2006 to May 31, 2008.
   f. Leslie-Anne Juarez (Undergraduate Research Student) – 100% Summer 2006.
   g. Kaycee Kloeppel (Undergraduate Research Student) 50% Fall 2006 and Spring 2007.
   h. Constance Lee (Undergraduate Research Student) – 100% Fall 2007.
   i. Marcos Lopez (Undergraduate Research Student) – 25% Spring 2006; 100% Summer 2006.
   j. Amber MacDonald (Undergraduate Research Student) - 100% January 15, 2007 to June 30, 2007.
   k. David Nelson (Subcontract Scientist) – 10% February 15, 2006 to November 30, 2006 (via Michigan Tech.) and December 1, 2006 to May 31, 2008 (via Univ. of South Alabama).
   l. Juliana Robles (Research Technician I) – 100% February 15, 2006 to July 31, 2006.

    m. Jonathan Scudder (Research Technician I) – 100% December 1, 2006 to November 30, 2007 and as a Consultant Dec. 1, 2007 to May 31, 2008.

    n. Vijaylaxmi (Subcontract Scientist) – 100% October 1, 2006 to December 31, 2006.

    o. Denise Wilson (Research Assistant) – 7% Spring, Summer, Fall 2006.

4. **Inventions/Patents/Discoveries:** None

5. **Collaborations/Consultants/Interactions:**

    a. Dr. Nancy J. Millenbaugh – Senior Scientist, General Dynamics, Advanced Information Systems, Brooks City Base, Texas 78235. Dr. Millenbaugh and the P.I. have a long association of research on MMW effects on cells, tissues, and animals. We have co-published work in the past.

    b. Dr. David A. Nelson – Professor of Mechanical Engineering and Chair, University of South Alabama, Mobile, Alabama. Dr. Nelson is developing a computational skin model of energy and heat transfer based on dimensional information provided by my research team. His primary approach to the problem is via FDTD (finite-difference time domain) algorithms. Dr. Nelson has a long history of collaboration with Dr. Mason.

    c. Vijaylaxmi, Research Scientist, Department of Radiation Oncology, University of Texas Health Science Center, San Antonio, Texas. 78229. Dr. Vijaylaxmi has collected a great deal of information concerning RFR damage to *in vitro* and *in vivo* exposures. She had an opportunity to analyze these data through a subcontract to this grant.

6. **Honors and Awards:**   None

7. **Key Findings/Results/Accomplishments:**

This research is an outgrowth of a previous AFOSR grant F49620-02-1-0372. The objective of the research was to build a model that can predict the heat response of a rat to continuously applied RFR at 35 and 94 GHz with a power density of between 50 mW/cm^2 to as much as 1W/cm^2. Previous modeling attempts have treated the skin and its immediate sub-environment as a homogenous slab. Skin, in reality, is layered, of varying composition, and under complex physiological control. The prime objective of this project was to build a model that better reflects the reality of the anatomy and physiology of skin.

The research paradigm is built around the rat model. Rat was used because it is a convenient research mammal and its size scales easily to the RFR transmitter equipment available at Brooks Citybase, Texas. During the course of the research, a dual 35/94 GHz transmitter that operates within the calibrated range of power densities of 50 to 100 mW/cm^2 was available to the

investigator. This transmitter was adjacent to an anechoic environmental chamber used for animal exposure. The 94 GHz transmitter that operates in the 1 W/cm^2 range was not able to this study.

The research followed four distinct paths: 1) defining skin thickness in the rat, 2) normalization of the temperature data, 3) the FDTD model, and 4) validity testing of the model. The report here is divided to reflect these four paths.

Protocol: animal handling, exposure, data collection, and tissue processing.
The description that follows appears in several papers that are in print, in press, in review, and in preparation. The animals involved in this study were procured, maintained, and used in accordance with the Federal Animal Welfare Act, the "Guide for the Care and Use of Laboratory Animals," and the experimental protocol was approved by the Trinity University Animal Care and Use Committee and by the Brooks Citybase Institutional Animal Use and Care Committee as ethically and scientifically sound. All RFR treated animals and related shams were maintained and exposed at Brooks Citybase and the animals used in ambient temperature experiments were housed and processed at Trinity University. All histological specimens were prepared at Trinity as well as the digital microscopy and image analysis.

Male Sprague Dawley rats (Charles River Raleigh) 3-4 months old and weighing 350-400 grams were used. The rats were housed individually in a standard polycarbonate solid-bottom cage with free access to water. Rats were fed a diet that maintained their weight between 350-400 grams. They were kept on a 12:12 hour light-dark cycle with room temperature maintained at 22-24°C.

The rats were initially anesthetized with 4.0% isoflurane, which was then maintained at 2.5% throughout the experiment using a calibrated rodent anesthesia system (IMPAC6, VetEquip, Pleasanton, CA). Under anesthesia, the left flank was shaved with electric clippers revealing approximately 13 % of the skin surface extending from the dorsal midline to the ventral midline thorax to pelvis. The right flank was not disturbed and served as a control. The hair was removed to allow for skin IR thermography.

Animals were placed on a Styrofoam platform in the exposure chamber lying on their ventral side with the shaved flank facing the RFR transmitter. Using a needle, a thermistor probe was centered on the shaved flank (2-3 mm in depth) to measure subcutaneous temperature. Another probe was inserted 5 cm into the colon to measure colonic temperature (body core). Both probes were secured with micropore tape on the tail. A probe fastened to the Styrofoam stand measured ambient temperature. The temperatures from the three probes were recorded using a LabVIEW software program (National Instruments, Austin, TX) installed on a Dell Inspiron computer. Surface temperature was measured with a FLIR Systems Indigo Merlin Infrared (IR) camera (Indigo Operations, Goleta, CA). The IR camera was calibrated with a MIkron Instruments Model M340 blackbody source (Oakland, NJ). The posterior legs and the left anterior leg were taped onto the platform to prevent any movement during exposure.

Rats were exposed to 60 minutes of continuously applied RFR at a frequency of 94 GHz or 35 GHz using a Millimeter Wave Exposure System (Applied Electromagnetics, Inc., Atlanta, GA). The ambient temperature in the exposure chamber was adjusted to 23°C with a humidity between 40 to 60%. Prior to exposure, the core body temperature of the anesthetized rat was maintained at 37.3°C, which was achieved by placing the rat on a heating pad. A three-minute control period was allowed to pass before initiation of exposure. Irradiation was conducted under far-field conditions with the animal centered along the boresight at 80 cm (at 94 GHz) from the antenna. After exposure, the area of maximal RFR exposure density was determined using the last image recorded by the IR camera and that site on the skin marked with a permanent marker. The right flank was then shaved, and an area similar to the one marked for the hot spot was marked. Anesthetized rats were euthanized by CO_2 asphyxiation.

The marked area plus 5 to 7 cm of surrounding tissue on the exposed left side and unexposed right side were harvested and fixed in 10% buffered formalin for 24 hrs. Tissue was processed (AFIP Lab. Methods in Histotechnology, short schedule, 1994) and embedded in paraffin (Fisher Paraplast) blocks. Blocks of tissue were chilled and cut into sections 6 μm in thickness using a microtome (Leica Model RM2235, Meyer Instruments, Houston, TX). The sections were then placed on microscope slides and stained using a general hematoxylin and eosin stain protocol. Digital images of prepared slides were collected using a 5 megapixel digital camera (SPOT Insight Camera 4, Diagnostic Instruments, Inc., Sterling Heights, MI) mounted to an Olympus

CX31 light microscope (Olympus America, Inc., Melville, NY). Image J, Adobe Photoshop, and Fovea Pro software was used in the analysis of the subsequent digital images. All physiological data was arrayed and analyzed using Microsoft Excel.

Path One: Defining skin thickness in rat.

Skin thickness can vary widely over the body. (See Waterson et al., 2005, J. Investigative Dermatology 124: 1078.) In the case of humans the integument can range from tenths of millimeters to a centimeter. The presence or absence of hair can affect the anatomy. Skin depth at a fixed point can change with the hair cycle stages, with age, and with diet. In constructing a thermal model for RFR-induced heat flow using a rat model, what skin anatomical conditions should be considered? To provide Dr. Nelson with average skin values for thermal modeling, a three dimensional skin depth map was created for the rat based on the treatment protocol described earlier. Figure One below represents the results of that effort.

The data for the image projections were produced by sampling the skin on the exposure surface at 1 by 2 cm intervals. (1 cm = dorsal to ventral; 2 cm = head to tail) One rat lateral skin side would yield from 56 to 69 sample blocks. These tissues were examined by microscopy and measured from recorded, calibrated digital images. Thermographs of RFR heat distribution of the skin at the end of exposure were superimposed on the calculated depths seen in figure one and the points of greatest correlation became the measurements for the standard rat skin in the thermal model. The standardized values used were as follows:

$$\text{epidermis} = 40 \ \mu\text{m};$$
$$\text{papillary dermis} = 100 \ \mu\text{m};$$
$$\text{reticular dermis} = 600; \text{ and}$$
$$\text{hypodermis} = 560 \ \mu\text{m}.$$

The dermis was separated into its two components due to both anatomical and physiological distinctions of the tissue. The thermal model was designed to accommodate this split. The hypodermis was defined as having 200 μm of fat, 200 μm muscle, and 160 μm connective tissue. The hypodermis could have more depth; however, the decision was made to limit the model to 1.3 mm in depth, a value that exceeds the RFR penetration value at the wavelengths employed. (See Eggers et al., 2003, 25th annual BEMS meeting.)
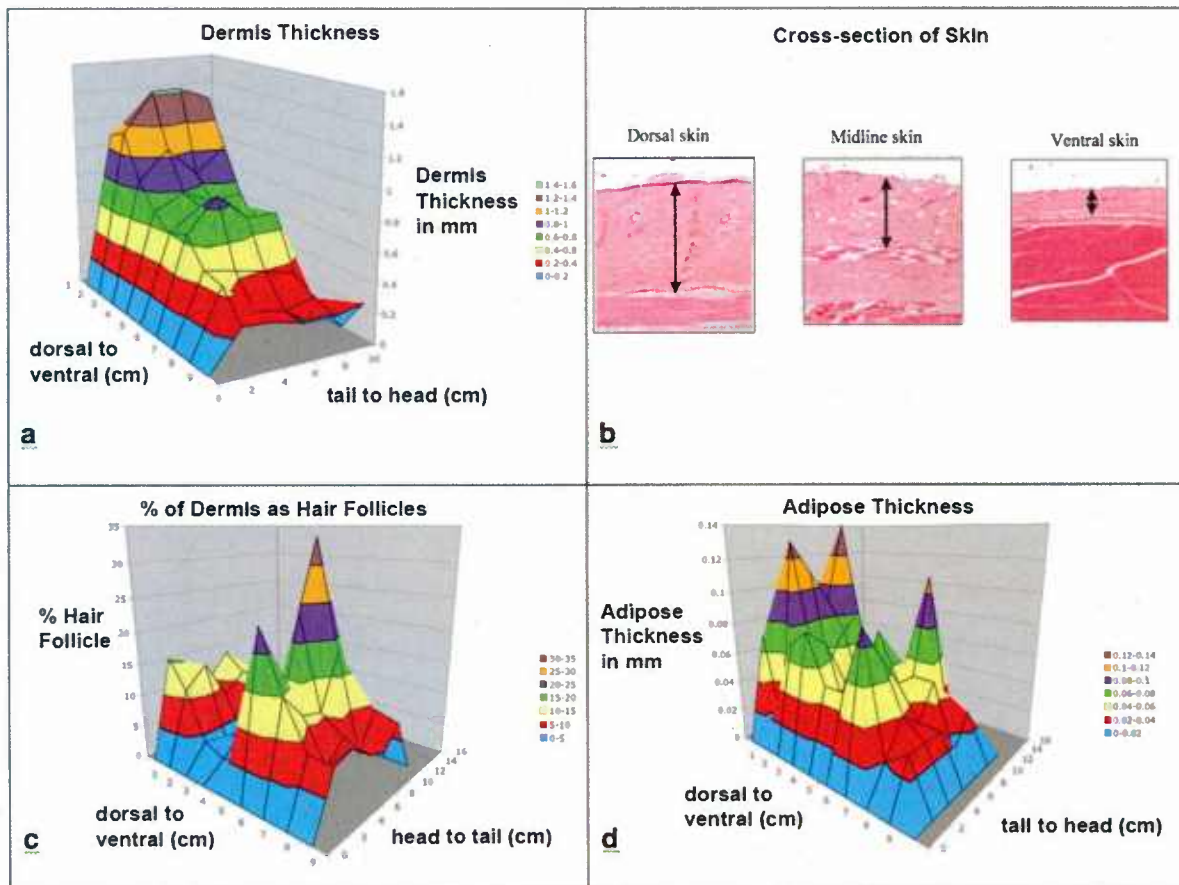
Figure One: Variation of rat skin thickness. Panel a represents dermal thickness over the flank of the rat (averaged for three animals). Coordinate 10,1 would be at head on back. Panel b displays histological cross-sections of the rat skin at three locations: at back (dorsal), lateral, and belly (ventral). Panel c shows the area contribution of hair follicles at different points of the flank skin. Coordinate 0,1 would be at head on back. Panel d represents the adipose thickness associated with the dermis and panniculus muscle at hypodermis interface. Coordinate 16,1 would be at head on back. Panel c projection is reversed to better show the data.
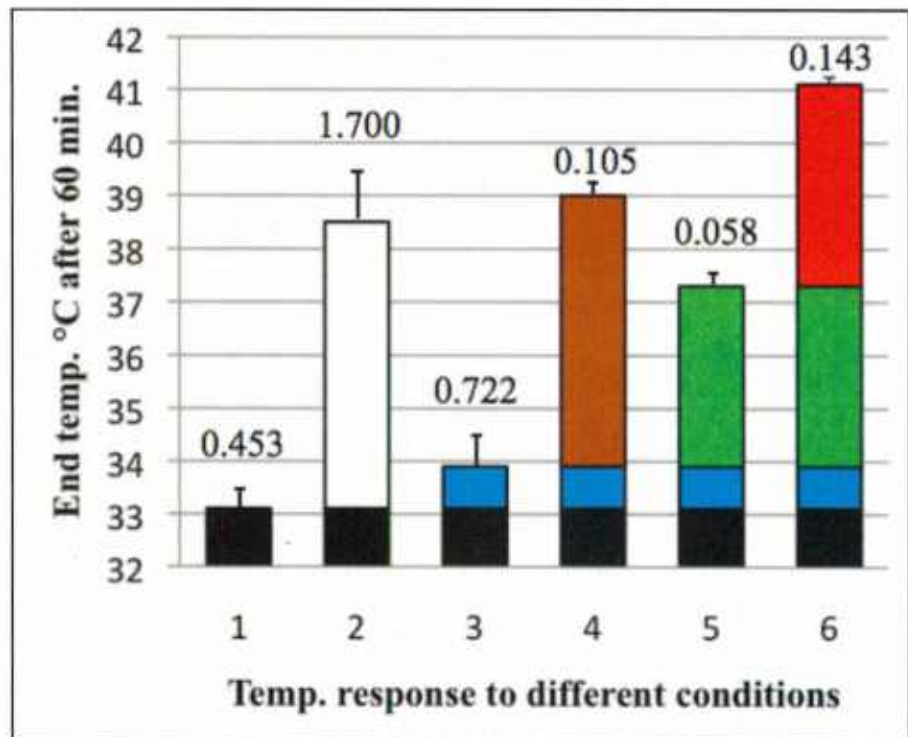
Path Two: Normalization of temperature data.

The ethical treatment of research animals that may suffer pain due to experimentation requires the use of anesthesia. Our study employed the respiratory anesthetic isoflurane. Anesthesia can produce hypothermia in both human and rat. (Sessler, 2000, Anesthesiology 92:578 and Gordon, 1990, Physiology and Behavior 47:963). Although both the control and RFR exposed animals were anesthetized, the degree to which the induced hypothermia affected "real" temperature values was unknown. Others have remarked about temperature depression in anesthetized

Grant number FA9550-06-1-0129

animals in strong fields, but rarely related the temperature decrease to anesthesia hypothermia (See Ichoika et al., 2003, BEMS Journal 24:380 for an example.)

The heat flow model could be affected in terms of whether the model accounts for anesthetic or whether the modeled animal is assumed conscious. It was therefore important to understand if the collected temperature data was significantly influenced by anesthesia hypothermia. A series of experiments was designed to investigate this possibility. A non-metallic, water-circulating heating pad was installed under the anesthetized animal in the exposure chamber. The pad was calibrated to hold the body core temperature of the rat to 37.3°C through a series of manually applied temperature "bumps".

Six conditions for temperature recording were developed: dead, sham (non-heat regulated), heat regulated, exposed dead, exposed non-heat regulated, and exposed heat-regulated. Therefore, the heat regulated anesthetized animal served as the surrogate for a conscious animal. The results of this experiment are seen in figure two.

Figure Two: End body core temperature after 60 minutes at 23°C for six treatment modalities with initial temperature of 37.3°C.
1 = end temperature of a dead rat (33.1°C);
2 = end temperature of a continuously RFR-exposed dead rat (38.5°C);
3 = end temperature for an anesthetized rat (33.9°C);
4 = end temperature of a continuously RFR-exposed, anesthetized sham rat (39.0°C);
5 = end temperature of a heat-supported

anesthetized rat (simulated conscious animal) (37.3°C);
6 = end temperature of a continuously RFR-exposed, heat-supported anesthetized rat (simulated conscious animal) (41.1°C).
Black = arbitrary baseline set to dead rat end temperature (33.1°C);

8

White = temperature difference of RFR-exposed dead rat and dead rat (5.4°C);
Blue = temperature difference between anesthetized sham rat and dead rat (0.8°C);
Brown = temperature difference between RFR-exposed anesthetized sham rat and anesthetized sham rat (5.1°C);
Green = difference between heat-supported anesthetized rat and anesthetized sham rat (3.4°C);
Red = difference between RFR-exposed, heat supported anesthetized rat and heat-supported anesthetized rat (3.8°C).
Standard deviation shown with n=3 for each treatment modality. Please note that the number two exposure was conducted at a power density of 75 mW/cm2 whereas all others were at 50 mW/cm^2.

The data indicated that the heat-supported anesthetized animal had a body core temperature after RFR exposure 2.1°C higher than the sham; however, the sham had a 1.7°C greater heat change from baseline than the conscious simulated animal. A power analysis indicated that the sample size was appropriate (n = 3) and a t-test indicated significance at $p > .005$. These results indicated that the validity check for the skin temperature flow model must reconcile whether the comparison data is for a conscious model or an anesthetized model.

These results suggested that a less aggressive way to regulate for anesthesia hyperthermia should be found. We reasoned that through ambient temperature control, the induced hypothermia could be cancelled without the difficult temperature bumping required by the external heating pad. At Trinity University we constructed a small environmental chamber where we could control the ambient temperature effectively.

Figure Three: At right, rat in temperature control chamber constructed at Trinity University.

In earlier work we had noticed that anesthetized rats held at 33°C ambient during RFR exposure demonstrated different heating patterns. Shams held at the higher ambient temperature did not demonstrate lower body core temperature with prolonged maintenance on isoflurane. A protocol was designed to measure the extent of anesthesia hypothermia temperature lowering as a

function of five-degree incremental ambient temperature differences. The practical value of the experimental design is that it might suggest that a conscious animal might respond differently to RFR in a real world environment. The results of that work are seen in figure four below.

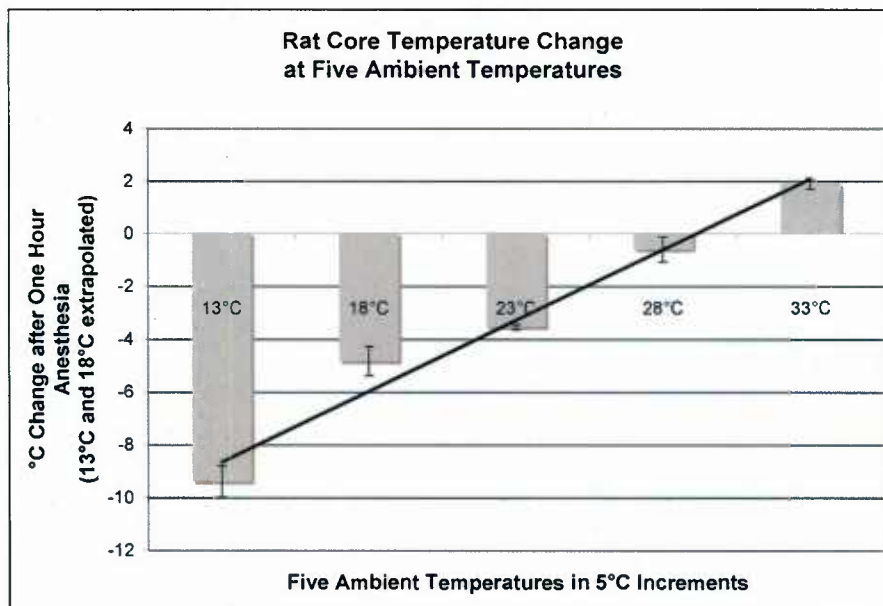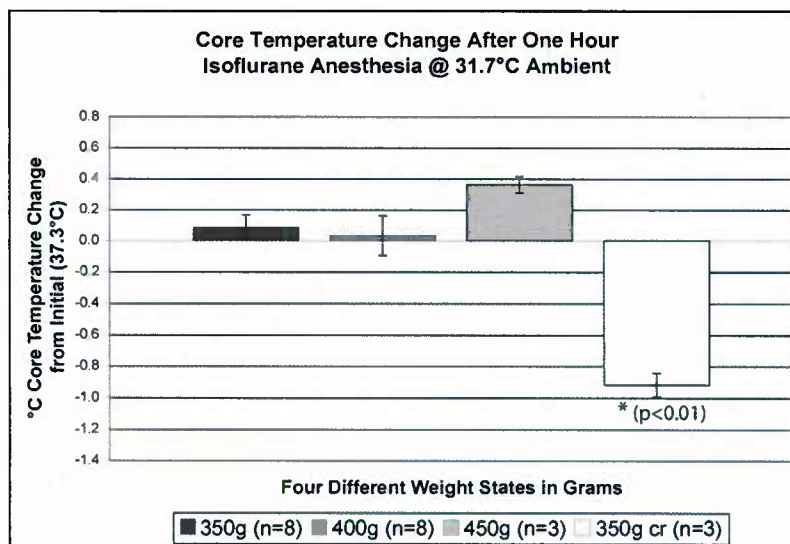**Rat Core Temperature Change at Five Ambient Temperatures**

Figure Four: Body core temperature change from 37.3°C after one hour of isoflurane anesthesia. N = 3 for each of five ambient temperatures tested: 13, 18, 23, 28, 33°C. Standard error shown. Mean rat weight 409 ± 20g.

The 13 and 18°C exposures put the animals into cold shock and the end point had to be extrapolated. The regression line suggested there would be an ambient temperature point at which an anesthetized animal would not demonstrate a hypothermic response. A temperature point was identified at 31.7°C and figure five represents that data.

Figure Five: Comparison of rat core temperature change from 37.3°C after one hour of isoflurane anesthesia for four weight conditions exposed to 31.7°C ambient. Four different animal weight states were examined. N = 3 for each weight state. cr = calorie restricted animal. The standard error is shown.

Core Temperature Change After One Hour Isoflurane Anesthesia @ 31.7°C Ambient

* (p<0.01)

Four Different Weight States in Grams

■ 350g (n=8) ■ 400g (n=8) ■ 450g (n=3) □ 350g cr (n=3)

This latter experiment explored several observations made during the course of this and the earlier bioeffects project. We noticed that heavier animals and calorie restricted animals seem to respond differently to RFR exposure. Male rats fed *ad libitum* will in time exceed 400 grams in weight. Our experimental protocol dealt with animals that ranged in weight from 350 to 400 grams. This weight range suggests an age for the laboratory rat. So by restricting the weight of the experimental animal, both body proportions and age are loosely defined. The experimental rats were ordered in lots of 20 or 40, depending on how fast data was to be collected. Some rats in a batch would, in time, exceed the imposed 400 gram limit and were subsequently calorie restricted. The calorie restricted animals appeared to behave differently in the RFR field. Figure 5 provides support for these observations. The first two animal groups (350 and 400 grams) did not demonstrate an anesthetic hypothermic response when held at 31.7°C ambient. Rats at 450 grams showed a slightly elevated response, but not significant. However animals that were calorie restricted from 400 grams back to 350 grams demonstrated a significant temperature response and were more likely to show a hypothermic response at 31.7°C than younger rats that reached the 350 gram threshold for the first time.

When these data are combined with the information found in figure 2, it suggests that weight, age, and calorie restriction could play a significant role in the RFR response under the exposure conditions explored in this work. Thermal modeling could investigate these variations further. In conclusion, a thermo-neutral ambient temperature (31.7°C) was discovered that would cancel anesthesia hypothermia in male rats. Research time was not sufficient to allow the RFR exposure testing at this anesthesia neutral temperature. We were able to define the skin dimensions for the thermal modeling work and suggest some physiological parameters that might be explored by the thermal models.

Path Three: The thermal modeling.
The thermal modeling work was performed in two stages: 1) while Dr. Nelson was at Michigan Technological University and 2) while he was at University of South Alabama. For the first stage model, a search of the literature provided information for SAR, permittivity, conductance, and depth. This information combined with the Pennes bioheat equation (Pennes, 1998, as

reprinted in Journal of Applied Physiology 85:5) yielded the working algorithm for this model.

Please see figure six below.

Figure Six:
The basic
formula for
thermal
flow in rat
skin.

$$\underbrace{k_t \nabla^2 T(x,t)}_{Conduction} + \underbrace{m_b C_b (T_a - T(x,t))}_{\substack{Convection \\ due \\ blood\ flow}} + \underbrace{q_m(x)}_{\substack{Metabolic \\ heat \\ generation}} - \underbrace{q_s(x,t)}_{\substack{RF \\ absorption}} = \underbrace{\rho_t C_t \frac{\partial T(x,t)}{\partial t}}_{\substack{Change \\ in \\ storage}}$$

Data elements in the initial thermal flow equation are represented, in part, by figure seven below.
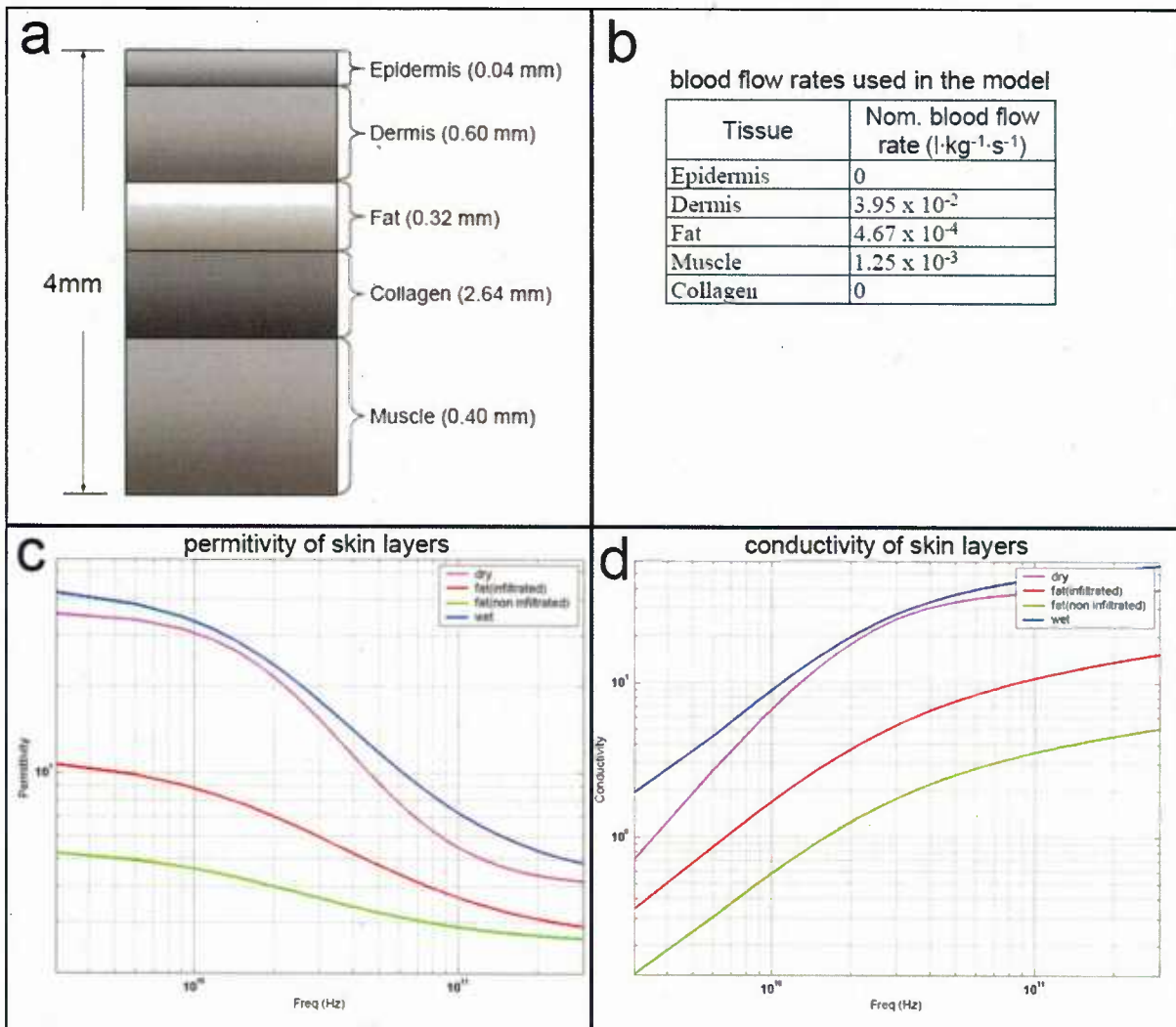

Figure Seven: Values for the first thermal equation. Plate a represents initial depth values for the study; plate b represent blood flow data; plate c provides permitivity data; and plate d describes conductivity data.

12

The sources of the values for figure seven were plate a = Blystone research data; plate b = Diller, 1985, in Heat Transfer in Biology and Medicine, Volume 2:85; and plate c and d = Gabriel and Gabriel, 1996, http://niremf.ifac.cnr.it/docs/DIELECTRIC/Report.html, especially Appendix B1. The depth data was not optimal, for example, dermis has collagen as well as the underlying connective tissue. There is fat both above and below the muscle tissue (panniculus). The depth of 4 mm is too deep considering the frequencies being used in this study. However, some initial values were developed to set into motion proof-of-concept and provide an initial comparison with actual physiological data. Of this initial effort figure eight provides the best fit between predicted and actual temperature flow in the epidermis.

Figure Eight: Comparison of FDTD predicted thermal data and actual experimental data for 94 GHz @ 75 mW/cm^2 continuous exposure of rat for 60 minutes at 23°C ambient temperature. Closed line is the modeled FDTD heat flow and the red squares represent the actual epidermal temperature changes as measured by IR thermography.
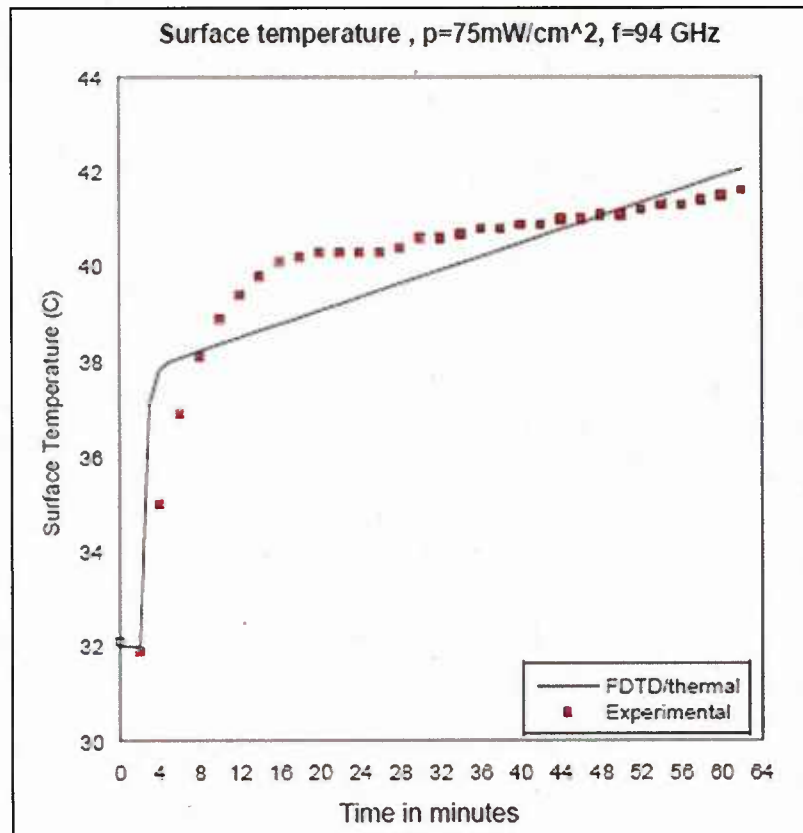
The model predicted a faster skin warm up than actual and then a steady heat load increase thereafter. More revealing was the comparison of the rate of temperature change. Once again the rate of change was far greater in the model by about two fold; however, the total increase in temperature was relatively accurate. Where the model diverges from actual was in the deeper

hypodermal layers. Actual subcutaneous temperature change was less than the model predicted as revealed in figure nine below.

Figure Nine: Comparison of rate of temperature change of 94 GHz, 60 minute continuous exposure, at 75 mW/cm^2 at 23°C ambient. A = model heat change with the slope calculated on a per <u>one-minute</u> basis. B = actual heat change with the slope calculated on a per <u>two-minute</u> basis. The A data is for depth distance not calibrated to skin structures. The B data is calibrated for body locations including the subcutaneous tissue and the colonic temperature.
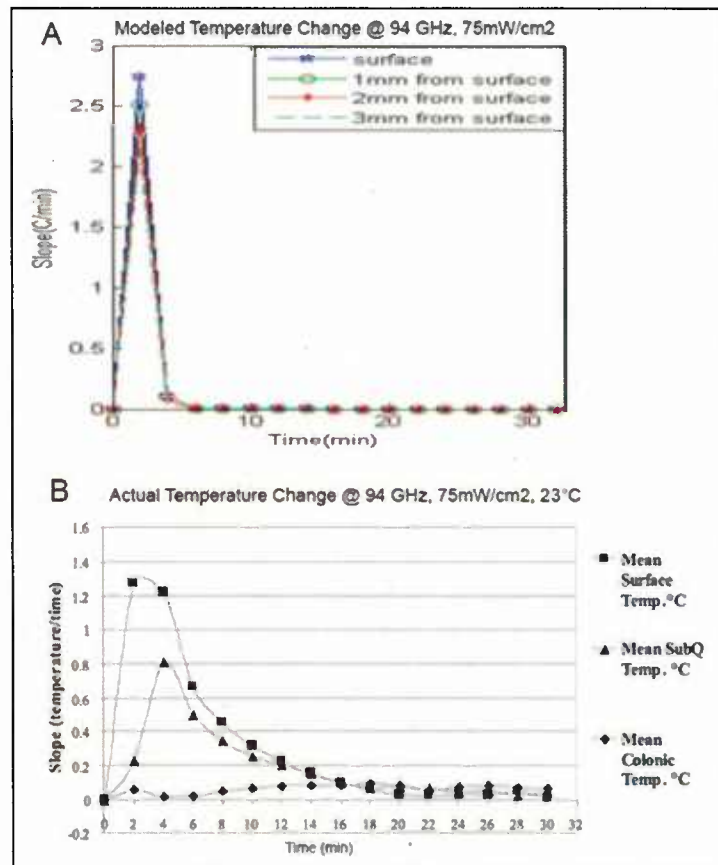
Overall the modeled curve data generally followed and complemented the actual data with the exception noted. After much deliberation, we made the following adjustments. 1) Rather than model thermal load 4 mm deep and at regular 1 mm intervals into the integument, the value 1.3 mm was chosen for the overall model depth. It was determined that the near surface blood vasculature would pull the heat away without significant heat diffusing to deeper levels of the hypodermis. 2) We decided to separate the dermis into two layers reflecting its anatomy. The papillary dermis is quite irregular and complements the interaction with the overlying epidermis. The vascular bed in the papillary dermis is different from that of the reticular dermis. The reticular dermis is more collagen laden than the papillary dermis. Hair follicle bulbs are a prominent feature of the reticular dermis along with sebaceous glands. The papillary dermis only has hair shafts and ducts coursing through it. 3) The new model reconfigured the hypodermis very differently, in part, because only the first 1.3 mm of depth would be considered.

Additionally our research data suggested we emphasize the panniculus carnosus muscle more in the model. Figure ten below provides support for the interest in this muscle layer.

Figure Ten: Rat dermis muscle interface exposed to 94 GHz at 23°C ambient continuously for 60 minutes. Different power densities are represented by the panels: panel A = 50 mW/cm^2; panel B = 75 mW/cm^2; panel C = 100 mW/cm^2; and panel D = 75 mW/cm^2. The ring in each panel indicates striated muscle referred to as panniculus carnosus muscle. The arrows indicate blood vessels at the interface that are extravasating blood cells.
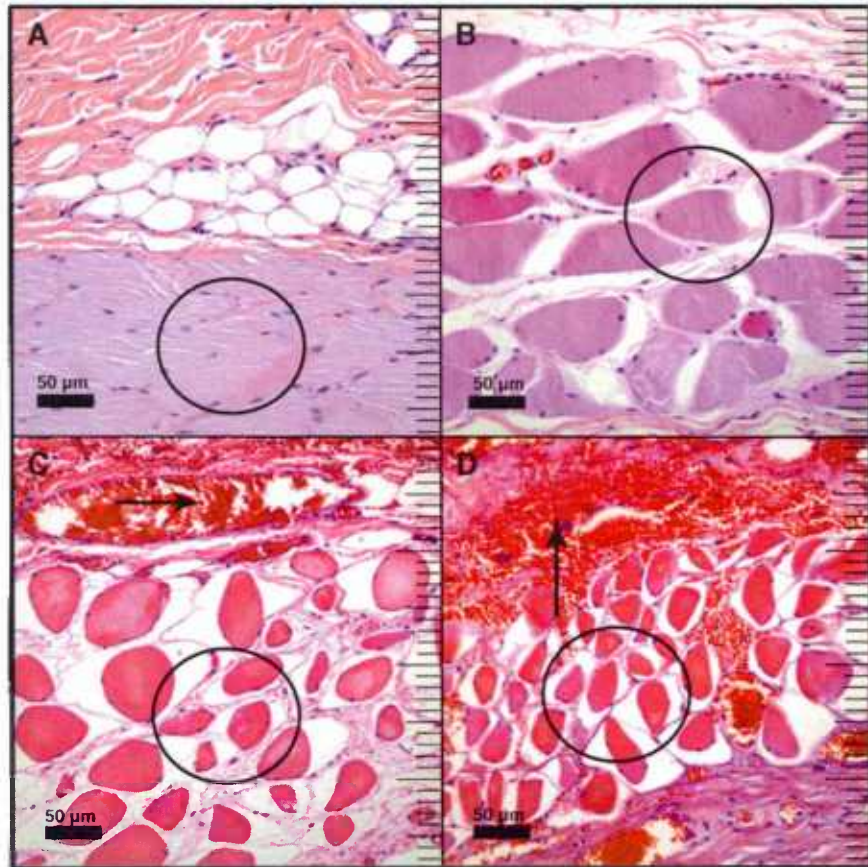

The RFR exposures indicated that one of the most sensitive areas to the millimeter wave energy was the muscle layer found at the interface between the dermis and hypodermis. Panels B, C, and D clearly show that the muscle fibers are pulling away from their endomysium when compared to the tissue in panel A. The panel A tissue compares favorably with control tissue.

A feature of mammalian anatomy is the panniculus carnosus muscle; however, in human anatomy many consider the only evolutionary remnant of this muscle to be the platysma of the throat and facial region. Fodor (1993, Aesthetic Plastic Surgery 17:179) provides an interesting review of the muscle as part of the superficial fascia system. Due to the apparent sensitivity of this muscle to RFR energy (see figure ten above), it is important to include this muscle into the revised thermal model. Figure eleven below provides insight into the difficulty of describing conditions for the model to include.

Figure Eleven: Digitally processed images of rat skin. <u>Left image</u> is a colorized histological section with green representing the dermis, yellow for fat cells, and red for panniculus muscle. The thin lavender strip at top is the epidermis. The <u>right image</u> is created for the FDTD data set and derived from the left image. Orange is dermis, red is fat, and blue is muscle. The black structures in the left image represent hair shafts.
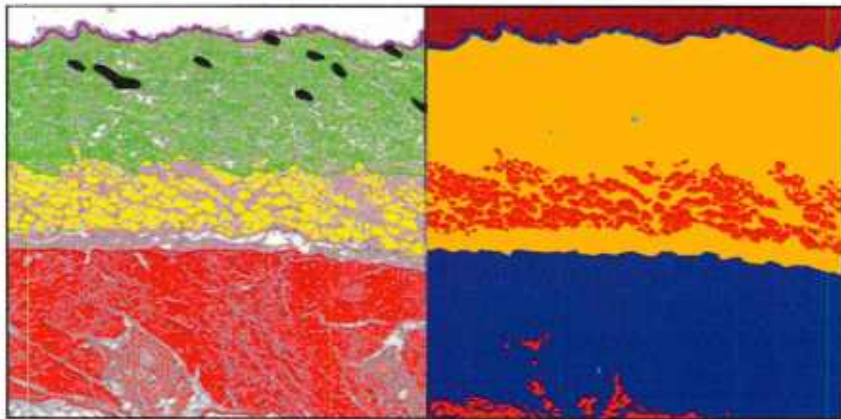
In some rats the flank side demonstrates no fat cells between the dermis and the muscle (more frequent with the absence of hair follicles). Less often there is little striated muscle tissue between the dermis and the fat laden hypodermis below. Made obvious in the right image, there is dermal tissue (orange) on both sides of the adipose layer (red). This second layer of dermis, or the dermal layer next to the hypodermis (and panniculus muscle), is where the largest blood vessels of the dermis reside; and the first vessels to demonstrate extravasation of blood cells with RFR heating. Some dermal tissue areas are occupied by expanses of hair follicles and shafts (as much as 25% of the area). Should the follicle areas be counted as dermis are questions to be addressed. The right image in figure eleven included the hair shafts in the dermis. A set of imaging "traffic rules" was followed when determining the skin dimensions put into the thermal transfer algorithm.

Figure twelve below represents the second stage skin thermal flow calculations. As has been mentioned the depth of tissue modeled was changed from 4.0 mm to 1.3 mm. The dermis was divided into two segments and enlarged to 700 μm in depth as opposed to the earlier 600 μm. The largest change was with the hypodermis by including much less of it in the equation. Given the variation of the location and thickness of both adipose and striated muscle (panniculus carnosus) the hypodermis was given a generalized location for these tissue masses; that is, they appear generally in the equation but not specifically as to location. Also rather than refer to collagen, the term connective tissue is used to better reflect histological terminology. Nervous system contributions to blood flow adjustment have yet to be added to the thermal equation.
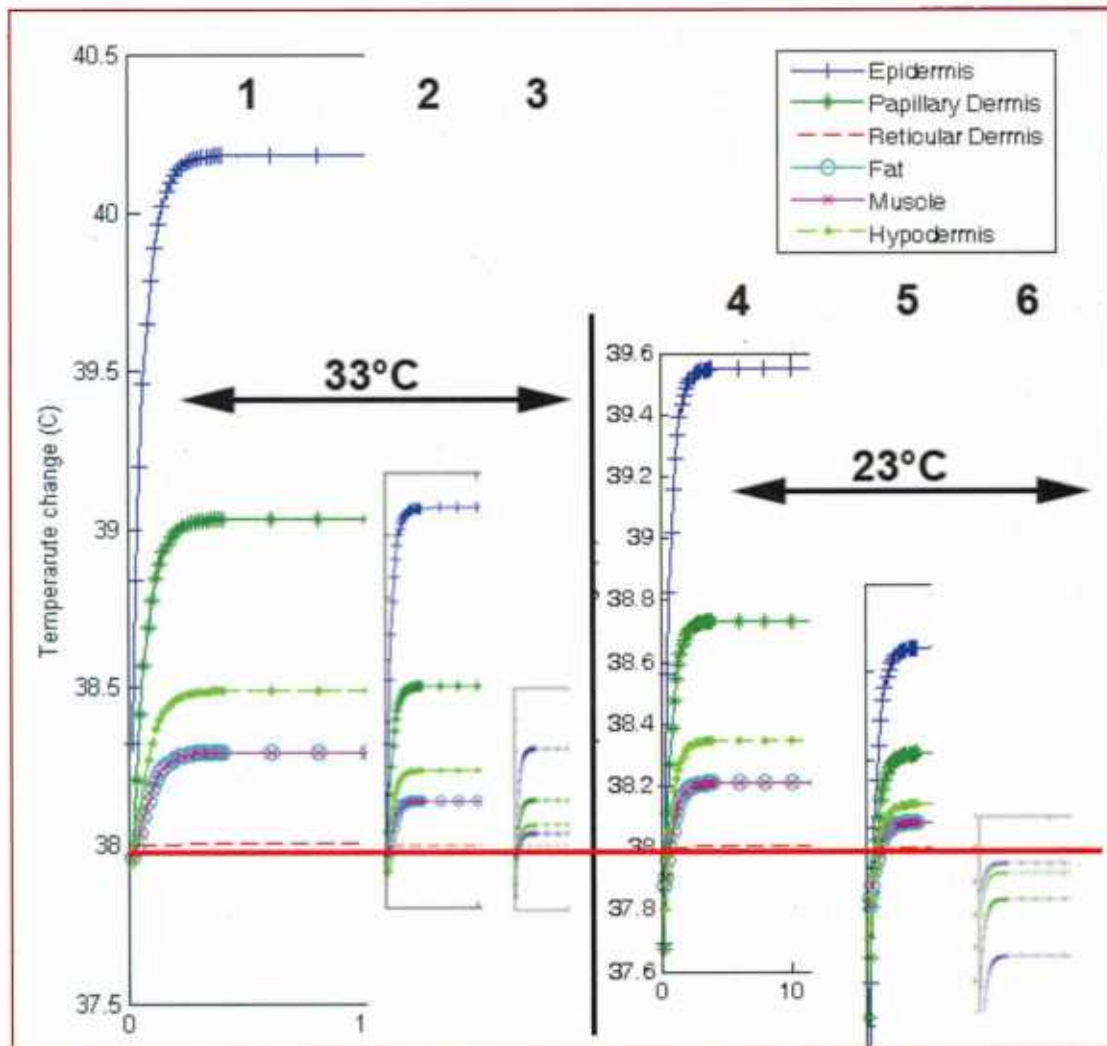
Figure Twelve: Thermal model predicting temperature elevation in rat for six exposure conditions to 94GHz @ 50, 75, and 100 mW/cm² delivered continuously for ten minutes at either 23 or 33°C ambient. Six graphs are combined into one figure with the "topside" numbers referring to each graph below the respective number: 1 = 100 mW/cm²; 2 = 75 mW/cm²; and 3 = 50 mW/cm². Graphs 1, 2, and 3 were all modeled at 33°C ambient. Continuing with the representation numbering, 4 = 100 mW/cm²; 5 = 75 mW/cm²; and 6 = 50 mW/cm². Graphs 4, 5, and 6 were all modeled at 23°C ambient. The horizontal red line represents a common temperature to all graphs, which have been scaled to be equivalent to one another on the y-axis (temperature). Also for the model the reticular dermis was held constant in temperature and at 38°C. The x-axis represents ten minutes intervals for each of the six graphs. Note: they are not of the same scale. Blue represents the center of the epidermis (consider as surface). Green is papillary dermis. Muscle and fat are considered together by blue circles on solid red line. The reticular dermis is the broken red line. The hypodermis is the broken green line. Muscle/fat are subsets of the hypodermis but shown independently here.

The positive element of the second stage thermal equation is that it better represents the heat flow by the layers of skin. The negative element is the equation does not deal with the slower temperature change after ten or so minutes of RFR warming under the conditions of the experiment. The grant funding time ended before this latter improvement in the equation could be affected.

Path Four: Validity testing of the model.

As has been mentioned earlier the rat as an experimental animal offers some interesting problems that must be addressed both in terms of developing appropriate skin layer dimensions for the thermal model and accounting for experimental handling of the laboratory animal. Perhaps the most interesting is how to deal with anesthesia hyperthermia. Clearly the thermal model will have the greatest utility when applied to a conscious life form such as a human. The anesthesia compensated rat attained a two-degree higher body core temperature with RFR exposure than the "usual" protocol treated animal. These compensated animals are also more likely to demonstrate skin lesions at the power density levels employed by this protocol. We also recognized that ambient temperature could influence the temperature response greatly to the point that it may be possible to cancel anesthesia hypothermia through the use of ambient temperature regulation (31.7°C in the case of the rat). These aforementioned elements impact the design and implementation of the constructed thermal model.

Figure thirteen, at right, reveals another interesting phenomenon. The percent amount of adipose in rat skin was surprisingly consistent in three of four weight conditions. When the rat passed a threshold weight, the percent adipose increased significantly. In other words, adipose gain is not linear in rat over a 100 gram range. These data call into
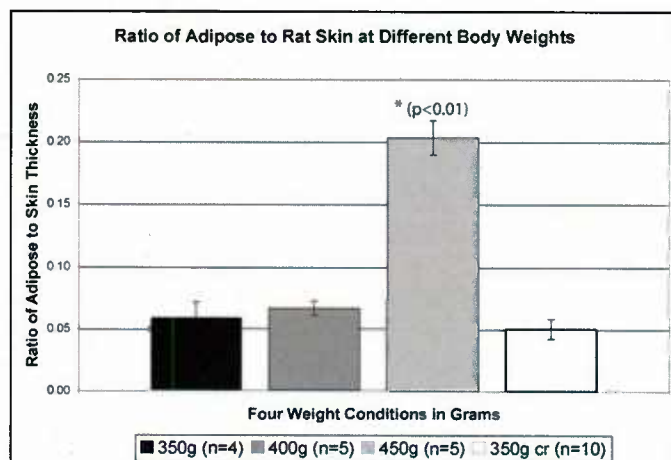

Figure thirteen: Ratio of adipose tissue associated with rat skin for different body weight conditions. Rats were sacrificed at specific weights at "n's" indicated on figure.

question how the insulating qualities of adipose tissue should be accounted for in the thermal equation. Correspondingly dermis values can change greatly for skin based on relative states of hydration that can occur naturally during a twenty-four hour period or under special dietary conditions. These issues all indicate that a set of physiological temperature data reflecting RFR exposure are subject to a great deal of interpretation just as the skin depth data is subject to interpretation.

The funding period for this project has ended. Dr. Nelson and I are continuing to refine the thermal heat transfer equation based on reams of collected data funded by both this project and the previous bioeffects grant. During the course of the next six months we expect to submit three additional papers for peer review. Ten Trinity undergraduate students have participated in this Air Force funded research project with six of them now in medical school.

8. Transitions/Technology Transfers: None